Experimental Evaluation and Quasi-dimensional Modeling of Hydrogen Combustion for Sustainable Maritime Applications

Nicole Wermuth*, Marcel Lackner, Markus Rossmann, Jan Zelenka
LEC GmbH, Inffeldgasse 19, 8010 Graz, Austria
e–mail: nicole.wermuth@lec.tugraz.at

Andreas Wimmer
Institute of Internal Combustion Engines and Thermodynamics,
Graz University of Technology

Michael Url, Wolfgang Fimml
INNIO Jenbacher GmbH & Co OG

ABSTRACT

The objectives of this study are to enhance the understanding of hydrogen ignition and combustion in large bore, high-speed engines and to develop a heat release model for hydrogen combustion in large bore engines that can be used for NO_x emissions predictions and 1D simulation-based performance optimization.

For this, experimental investigations of hydrogen combustion were performed on a single-cylinder large bore research engine featuring an open chamber combustion concept with spark ignition and port fuel injection. Quasi-dimensional modeling was based on well-established natural gas open chamber combustion models and hydrogen combustion properties, like laminar flame speed. Data from the experimental investigations were used for model adjustments and refinement and to validate the predictability of the developed model.

Potential improvement areas of the hydrogen combustion concept, particularly with regard to the hydrogen ignition and early combustion phase will be presented and the validity and limitations of the developed heat release model will be assessed.

KEYWORDS

Sustainable combustion, hydrogen, combustion modelling, internal combustion engine, sustainable shipping

INTRODUCTION

Transoceanic shipping is very important for international trade, has high energy efficiency per ton and kilometer, and it is expected to increase significantly in volume in the future. The International Maritime Organization adopted a resolution in April 2018 to reduce greenhouse gas emissions by at least 50 % by 2050 compared to 2008 [1]. In order to meet this goal, there is a need to consider new fuels and innovative technology solutions. The HyMethShip project (Hydrogen-Methanol Ship propulsion using on-board pre-combustion carbon capture) – a cooperative R&D project funded by the European Union's Horizon 2020 research and innovation program - aims to drastically reduce emissions and improve the efficiency of waterborne transport at the same time [2]. The HyMethShip system targets a reduction in CO_2 of more than 97 % and will practically eliminate SO_x and PM emissions. NO_x emissions will

* Corresponding author.

be reduced by more than 80 %, significantly below the IMO Tier III limit. The drastic CO_2 reduction is a result of combining methanol steam reforming, a CO_2 capture system, as well as a hydrogen-fueled combustion engine into one system.

In the HyMethShip concept engine exhaust gas enthalpy is used to provide heat to the methanol steam reforming process which in turn produces the hydrogen for the engine combustion. This interaction results in a rather unique set of requirements for the engine combustion system. Like in other engine applications high efficiency and low engine-out NO_x emissions are desired. In addition, there are requirements for engine exhaust gas temperature and exhaust enthalpy flow rate. The amount of hydrogen that is available for combustion is directly linked to the useful heat that can be extracted from the engine exhaust gas. Common NO_x emission reduction strategies like an increase of the excess air ratio (EAR) might not be feasible in the HyMethShip concept because high dilution of the combustion mixture could result in unacceptably low exhaust gas temperatures.

In a previous study [3] a hydrogen open chamber combustion concept was developed and experimentally validated in a single-cylinder research engine. For further optimization of the operating range and the engine efficiency but particularly for the optimization of the combined reformer-engine system a simulation approach is considered most promising. One critical feature of a HyMethShip system model is a combustion model that is able to predict the HRR as well as NO_x emissions and exhaust gas temperature. The development of a quasi-dimensional hydrogen combustion model for a large-bore high speed engine will be the focus of this study.

Apart from the challenging boundary conditions and constraints the combustion system experimental evaluation was also hampered by high cyclic variability and individual combustion cycles with extremely early or extremely late combustion. This behavior seemed more pronounced than in similar engines operating with different fuels and fuel mixtures.

Recent studies examined the effect of hydrogen addition to conventional and alternative fuels. Kim et al. [4] investigated a turbocharged gasoline direct injection (DI) engine with a displacement of approximately 2 L and a compression ratio (CR) of 9.5:1. An energetic hydrogen share of up to 5 % led to improvements in cycle-to-cycle variations as well as in thermal efficiency.

Tutak et al. added [5] hydrogen to the natural gas (NG) flow of an NG-Diesel-Dual fuel (DF) engine operated at an indicated mean effective pressure (IMEP) of 7 bar and engine speed of 1500 rpm. Hydrogen addition decreased the combustion duration by 30 % while peak temperature and pressure increased. This resulted in an increase in NO_x emissions. Cycle-to-cycle variations and knocking set the limit of the hydrogen energy fraction of 19 %.

Another experimental investigation was carried out by Yu et al. [6]: Gasoline port fuel injection (PFI) was combined with hydrogen DI. Pure gasoline, gasoline plus homogeneously mixed hydrogen and gasoline plus stratified hydrogen operation were compared to each other. Fuel stratification led to a more stable and faster ignition and also to a faster subsequent combustion. Thermal efficiency but also NO_x and HC emissions increased because of a higher hydrogen content near the spark plug and less hydrogen close to the wall.

Hydrogen combustion was not only investigated experimentally but also with the help of simulations. Sapra et al. [7] used measurement data of a turbocharged spark-ignition (SI) marine gas engine to develop a 0D combustion model which was used as a basis for Seiliger and Double-Wiebe combustion characterization of several hydrogen-NG fuel blends at different engine loads. It was found that the Seiliger model was able to capture the effects of hydrogen addition on the combustion process at different loads while the Double-Wiebe model is suited for capturing the late burn phase of lean-burn NG and hydrogen-NG combustion.

Mixtures of hydrogen and other fuels, i.e. methanol, ethanol and methane, were used by Zhen et al. [8] in 1D simulations of a conventional diesel engine modified for methanol

operation. By adding hydrogen, the ignition delay (ID) and the combustion duration increased. The same trend applies for HC and NO_x while CO and CO_2 emissions were reduced.

Another simulation approach is described by Tüchler and Dimitriou in [9]. 1D engine simulations of a 5.2 L hydrogen-diesel DF engine operating at 1500 rpm were carried out. Calculation of the laminar flame speed (LFS) needed by the predictive dual fuel combustion model used was done with a Python script linked to the combustion model. Experimental validation was limited to a maximum energetic hydrogen share of 57 %. Engine operation with pure hydrogen fueling was not possible for either engine load condition or diesel injection strategy investigated.

Overall no clear trends of combustion stability and combustion and ignition duration with the addition of hydrogen have been reported. No detailed investigation is available for pure hydrogen operation in large bore engines.

In this study the experimental evaluation of hydrogen combustion including engine testing and data processing is described that is the foundation for the model development and detailed analysis. Subsequently, the chemical kinetics calculations as well as the 0D and 1D simulations are outlined. Special emphasis is laid on the combustion model and its adjustment for hydrogen combustion. Afterwards, selected experimental and simulation results are presented. Finally, potential improvements of the combustion system and the modeling approach are discussed.

METHODS

Experimental approach

Engine testing. The experimental investigations were carried out on a high-speed 4-stroke single cylinder engine (SCE). For these tests the engine was used in an open chamber configuration with a centrally mounted spark plug. The compression ratio (CR) was chosen in the range of typical gas engine applications with low flashpoint fuels and a camshaft with early intake valve closing (IVC) before bottom dead center was selected.

Table 1 shows further information about the engine. The hydrogen was admitted to the engine via PFI. For this, a modified serial production gas dosage valve and an injection nozzle design – investigated with 3D CFD prior to the engine testing – were used. Figure 1 shows a computer-aided design (CAD) model of the assembly of the nozzle and the intake ports.

Table 1. SCE technical data

Rated speed	1500 rpm
Displacement	≈ 6 dm^3
Compression ratio	Adjustable by modifying the piston geometry
Valve timing	Miller valve timing with early IVC, adjustable by modifying cam lobe profile
Number of intake and exhaust valves	2/2
Swirl/tumble	≈ 0/0
Charge air	Provided by external compressors with up to 10 bar boost pressure
Hydrogen supply	Port fuel injection, up to 10 bar
Ignition system	Modified high-voltage capacitor discharge ignition system
Balance of inertia forces	Lancaster mass balance for first and second order inertia forces

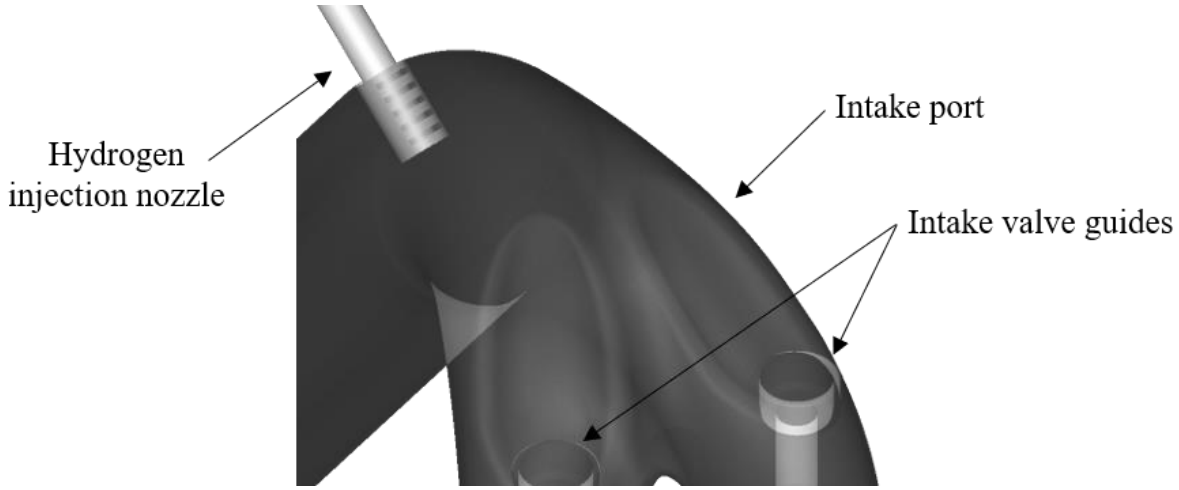

Figure 1. Position of the hydrogen injection nozzle in the intake port

All engine fluids including cooling water, lubricating oil, fuel gas and charge air are controlled to ensure well-defined and reproducible testing conditions. Instead of a turbocharger, an air compressor upstream of the engine and a flap in the engine exhaust system are used to adjust intake and exhaust manifold pressures. A flush mounted piezoelectric cylinder pressure transducer enables real-time calculation of the IMEP of each cycle. Additional measuring instruments are shown in Table 2.

Table 2. SCE measurement instrumentation

Quantity	Instrumentation
Air mass flow	Emerson Micro Motion CMF300
Hydrogen mass flow	Emerson Micro Motion CMF050
Charge air humidity	Vaisala HMT 338
Charge air temperature	Resistance temperature sensor PT100
Charge air pressure	Piezoresistive pressure sensor
Cylinder pressure	AVL piezoelectric transducer QC34C
Exhaust gas temperature	Thermocouple type K
Exhaust gas pressure	Piezoresistive pressure sensor
Exhaust gas emissions	V&F HSense, IAG FTIR, AVL AMA i60

During the SCE investigations the key operating parameters, i.e. EAR and ignition timing (IT), were varied for selected IMEP at a constant engine speed of 1500 rpm to study their impact on combustion, emission formation and operating range of the engine. The EAR is determined from the measured air and fuel mass flow rates ($\dot{m}_{\mathrm{L}}$ and $\dot{m}_{\mathrm{B}}$) and the stoichiometric air-to-fuel ratio L_{st}:

$$EAR = \frac{\dot{m}_{\mathrm{L}}}{\dot{m}_{\mathrm{B}} \cdot L_{\mathrm{st}}}, \tag{1}$$

The EAR was varied in the range from 1.75 to 3.0 by adjusting the boost pressure. Exhaust gas pressure was set according to 1D simulation results. IT was modified between 50 and 5 crank angle degree (CAD) before top dead center (TDC). Based on 3D CFD simulation results the end of injection (EOI) and the maximum injection duration of the hydrogen was set to 90 CAD after TDC (gas exchange) and 80 CAD, respectively.

Data processing. Heat release analysis was performed using the in-house simulation and analysis tool LEC CORA (**C**ombustion **O**ptimization, **R**esearch and **A**nalysis), crank angle resolved in-cylinder pressure data and additional measurement quantities like the gas composition. For a detailed analysis of the engine operation on the test bed heat release rates (HRR) for each individual engine cycle are produced, along with the key metrics mass fraction burned 5 % (MFB5%), MFB50% and MFB90%. An average HRR for 60 consecutive engine cycles is calculated as an input for the 0D combustion model development.

Modeling approach

The modeling approach combines 1D performance simulations with 0D combustion simulations based on an in-house open chamber combustion model (OCM). Additionally, chemical kinetics simulations were performed to provide LFS data for the 0D combustion simulation.

Chemical kinetics. The 0D combustion model relies on accurate laminar flame speed data. Several models for laminar flame speed calculations have been used in the OCM in the past but none of them had been validated for hydrogen combustion. The model developed by Peters [10] is suitable for hydrogen but was mainly used for near-stoichiometric mixtures in the past. An initial assessment showed that for the pressure (p) and EAR conditions encountered in the cylinder the laminar flame speed calculated by the model was too low. Therefore, LFS was calculated with the chemical kinetics software Cantera [11] and tabulated for use in the OCM simulation.

The calculation of laminar flame speed in Cantera is based on the progression of a "free-flame" through its environment consisting of a homogeneous mixture with a given EAR, pressure, and temperature (T) far away from the flame front in the unburnt mixture. Laminar flame speed was calculated with several reaction mechanisms for various temperatures and EAR. The results were evaluated based on laminar flame speed data available in the literature. The USC 1 reaction mechanism [12, 13], consisting of 14 species and 32 reactions and developed specifically for H_2/CO mixtures, offered the best trade-off between accuracy, computational cost and stability. For the laminar flame speed tabulation, the thermodynamic properties of the mixture, i.e. pressure, temperature and EAR, have to be representative of the in-cylinder conditions of the engine. To avoid extrapolation during the 0D combustion simulation the range in which each parameter was varied was selected to cover all in-cylinder conditions over the whole engine operating range. The ranges as well as the number of sampling points can be seen in Table 3. Overall, 50,000 data points were tabulated. The validation, however, was limited to ambient pressure and slightly elevated temperatures due to a lack of published experimental data for typical in-cylinder conditions.

Table 3. Parameter variation for the calculation of the LFS

Parameter	Lower limit	Upper limit	Sampling points
p/bar	1	150	50
T/K	280	1200	50
EAR/-	1	4	20

0D combustion simulations. The OCM is based on the flame front modeling of Auer [14] and incorporates models for the turbulent flame speed and turbulence according to Zimont [15] and Bargende [16], respectively. The OCM is used to describe premixed combustion in open chamber combustion engines where the combustion chamber can be divided into three zones (Figure 2):

- Burned zone
- Unburned zone
- Flame front

Combustion or flame front propagation is described as mass transfer between the different zones. The OCM considers the in-cylinder flow field and the combustion chamber geometry and consists of several sub-models to describe flame entrainment, the flame front, squish flow and turbulence. In this chapter the model attributes that have been modified for the hydrogen engine application via the model parameters $C_{\mathrm{mod}}, C_{\mathrm{k}}, C_{\mathrm{L}}, C_{\mathrm{ID}}$ are discussed. Further details can be found in [14].

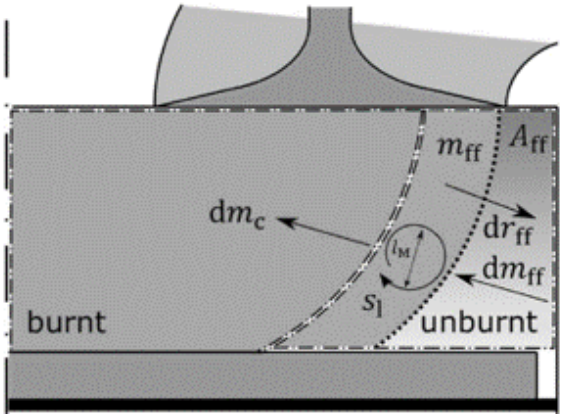

Figure 2. Division of the combustion chamber in zones

The mass flow from the flame front into the burned zone is calculated as

$$\mathrm{d}m_{\mathrm{c}} = C_{\mathrm{mod}} \cdot \frac{m_{\mathrm{ff}}}{\tau}, \tag{2}$$

where $\mathrm{d}m_{\mathrm{c}}$ is the change of mass of the burned zone, C_{mod} is a model parameter and m_{ff} and τ are the mass in the flame front and the characteristic burn duration, respectively. The turbulent kinetic energy k_{ivc} at IVC inside the combustion chamber is determined by the entry velocity w of the fuel-air mixture and is calculated as follows:

$$k_{\mathrm{ivc}} = C_{\mathrm{k}} \cdot \frac{1}{2} \cdot w^2. \tag{3}$$

C_{k} is a model parameter. The change of the turbulent kinetic energy is dependent on the change of the cylinder volume and the integral length scale, which is calculated as

$$l_{\mathrm{I}} = C_{\mathrm{L}} \cdot \sqrt[3]{\frac{6V}{\pi}}, \tag{4}$$

where l_{I} is the integral length scale, C_{L} is a model parameter and V is the instantaneous cylinder volume. Another important parameter with impact on the combustion is the ID. In the OCM the ID is modelled as a decelerated transition from a laminar to a turbulent flame. The flame speed s_{t} is given by

$$s_{\mathrm{t}} = \min\left(s_{\mathrm{l}} + (s_{\mathrm{t0}} - s_{\mathrm{l}}) \cdot C_{\mathrm{ID}} \cdot \frac{2r_{\mathrm{fr}}}{l_{\mathrm{I}}}, s_{\mathrm{t0}}\right). \tag{5}$$

s_l and s_{t0} are the laminar flame speed and turbulent flame speed, respectively, C_{ID} is a model parameter and r_{fr} is the vertical major axis of the ellipsoid the flame front is generally described as.

The model parameters C_k and C_L are linked to physical effects that are dependent on combustion chamber geometry and operating parameters, and have to be adjusted for every engine type and operating condition. The factors C_{mod} and C_{ID} are linked to the fuel dependent effects ignition and combustion and have to be adjusted for hydrogen operation.

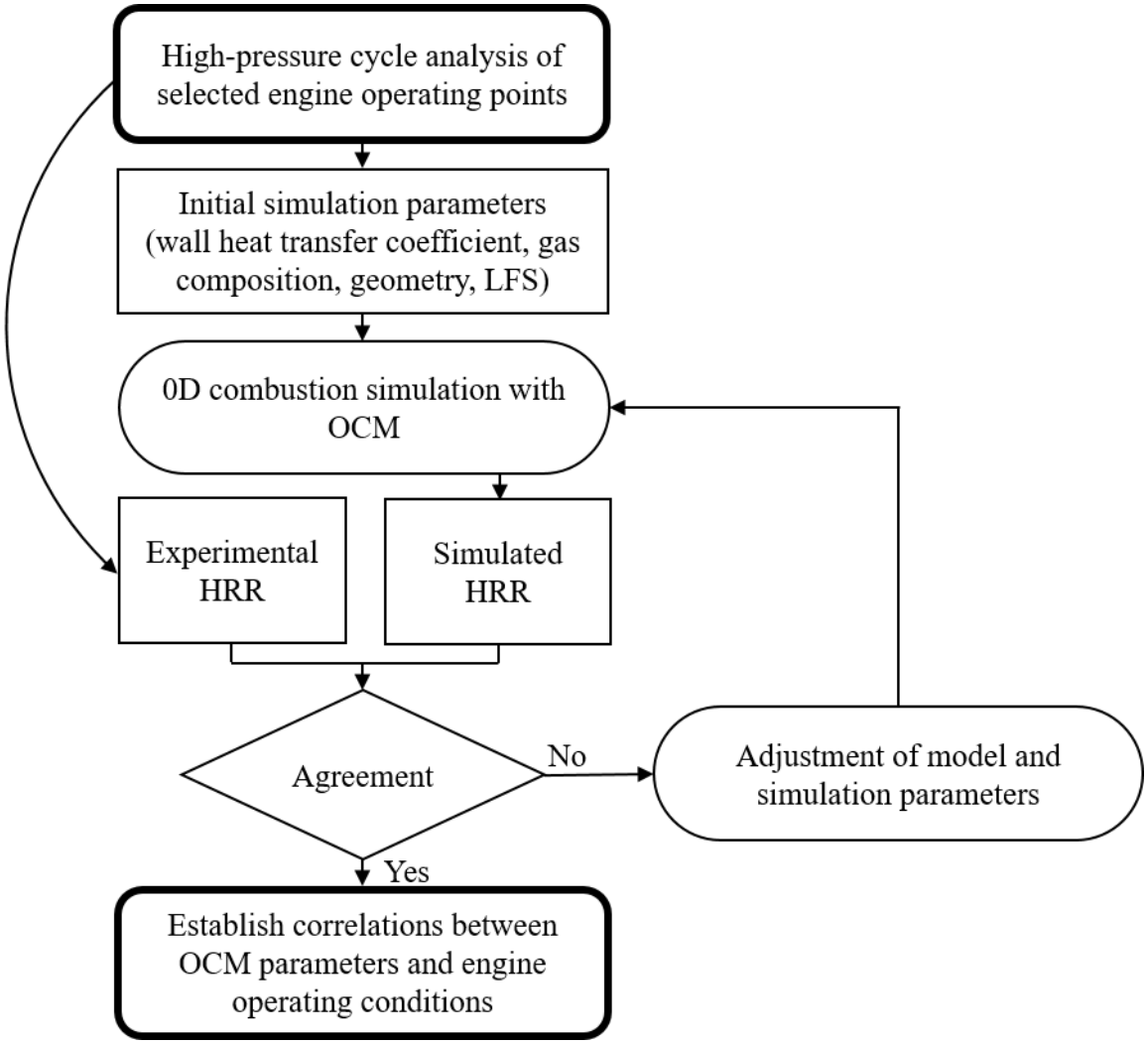

Figure 3. Flow chart of the 0D combustion simulation procedure

In Figure 3 the simulation procedure is shown. The simulation parameters consist of results from the measurement analysis, e.g. wall heat transfer coefficients, gas compositions and engine geometry, and the LFS tables. The HRR calculated by the OCM simulations are compared to the experimental HRR based on an assessment of the entire combustion phase. The adjustment of model parameters is performed based on the least squares method and the additional constraints for deviations from measured IMEP, NO_x emissions, MFB50% and in-cylinder temperature at the opening of the exhaust valve listed in Table 4. Finally, correlations between OCM parameters $C_{mod}, C_k, C_L, C_{ID}$ and engine operating conditions, e.g. IMEP, EAR and IT, were established.

Table 4: Constraints for model parameters adjustments

Parameter	Allowed deviation from measurement
IMEP	± 0.5 bar
NO_x	± 30 ppm
MFB50%	± 1.0 CAD
T_{EVO}	± 25 K

In the following the results of the adjustment of the OCM parameters presented in equations (2) – (5) is described.

- Integral length scale factor C_L

The integral length scale represents one relevant geometrical dimension of the engine. The impact of the integral length scale factor on the simulated HRR can be seen in Figure 4. In a first step a simultaneous rough adjustment of all four model parameters (including the integral length scale factor C_L), was performed for the maximum engine power operating condition. A value of 0.06 yielded the best results. Since the dimensions of the engine are constant across its operating range and the change of cylinder volume during the cycle is considered in the model, C_L was kept constant for other engine load conditions.

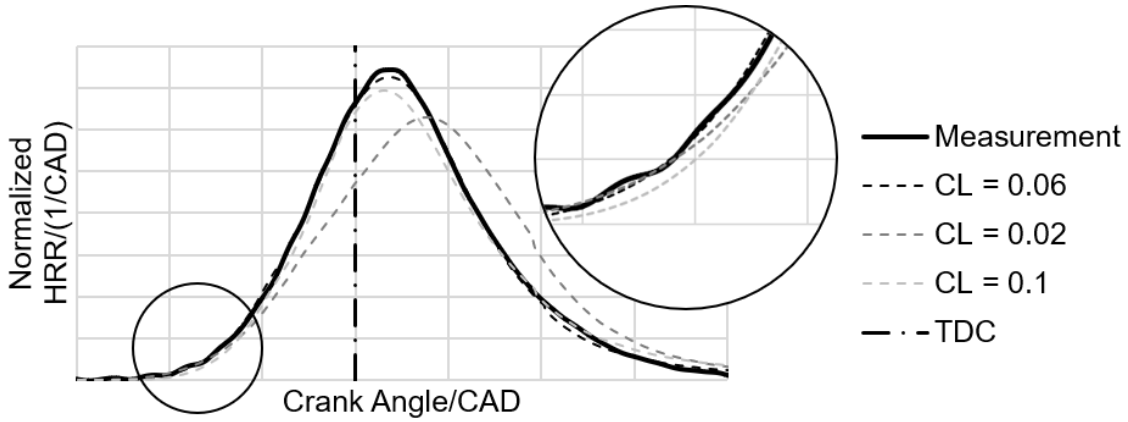

Figure 4. Influence of the integral length scale factor C_L

After C_L was set the other three model parameters were adjusted in a second step where varying engine operating conditions were considered.

- Turbulent kinetic energy factor C_k

The turbulent kinetic energy factor C_k is a modifier of the initial value of the turbulent kinetic energy at IVC. Evaluation over a larger engine operating range showed a strong dependence of C_k on the trapped mass in the cylinder (see Figure 5, left). At high EAR and IMEP, equivalent to high trapped mass, there was a large variance in C_k that could not be represented by the trapped mass alone. Detailed analysis showed that especially at high EAR higher C_k values were required to achieve a good agreement between experimental and simulated HRR. Therefore, EAR was introduced as an additional parameter into the expression for C_k. Figure 5 (right) shows the dependency of C_k on EAR and trapped mass.

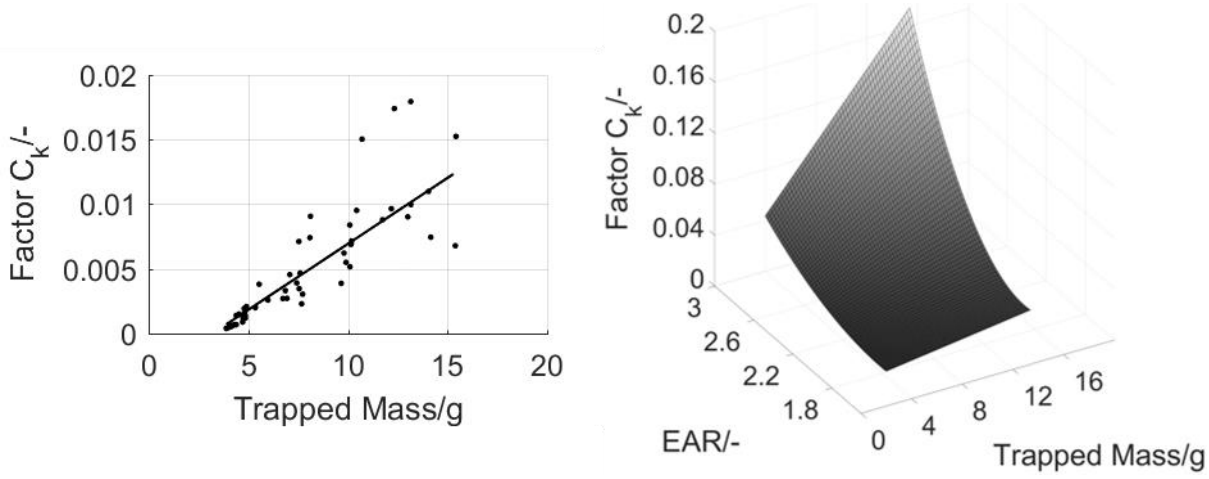

Figure 5. Dependency of the turbulent kinetic energy factor C_k on trapped mass (left) and final correlation between C_k and EAR and trapped mass (right)

- Ignition delay factor C_{ID}

The ignition delay factor C_{ID} directly influences the early ignition and combustion phase. Because of the impact of the early combustion phase on the subsequent main combustion (cf. "Experimental results") the adjustment of C_{ID} also has to consider the entire HRR using the least square method.

C_{ID} did not show a strong dependence on IMEP and a function was established reflecting C_{ID} dependency on IT (linear) and EAR (cubic) (Figure 6). Physical effects like temperature and mixture inhomogeneities in the combustion chamber or cyclic variabilities are not reflected in the combustion model and introduce some uncertainties to the model predictions.

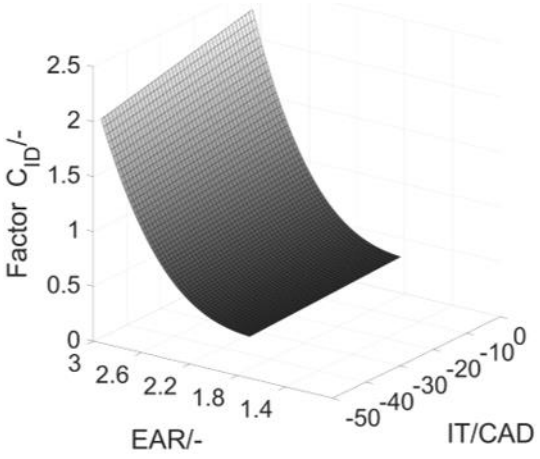

Figure 6. Dependency of the ignition delay factor C_{ID} on EAR and IT[†]

- Combustion factor C_{mod}

One of the key parameters influencing the mass transfer into the burned zone and therefore the main combustion velocity is the laminar flame speed that varies with pressure, temperature and EAR. C_{mod} is used to modify the mass transfer into the burned zone if the calculation based on the laminar flame speed fails to accurately reproduce the trends from the experimental assessment. Analysis of the combustion factor C_{mod} over the engine operating range showed that

[†] A negative sign indicates crank angle positions before TDC.

particularly at high temperature and pressure conditions for very high EAR larger corrections are required. For these operating conditions the laminar flame speed calculation was not validated due to the lack of experimental data (see "Chemical kinetics") and might be the cause of larger deviations. The combustion factor C_{mod} was finally described as a function of EAR and IMEP (Figure 7).

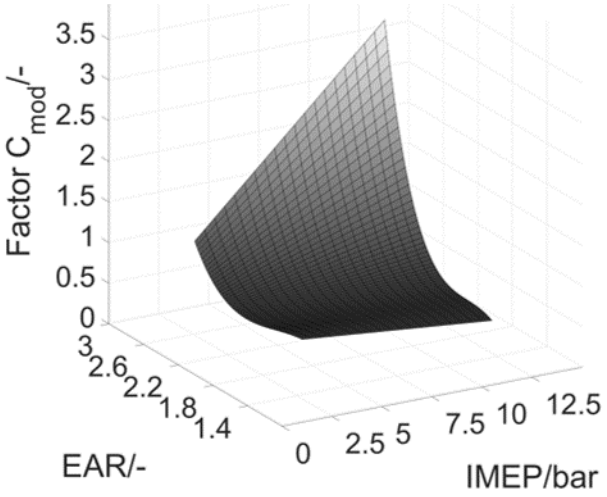

Figure 7. Dependency of the combustion factor C_{mod} on EAR and IMEP

1D engine simulations. Engine performance simulations were performed using the 1D simulation tool GT-Power. The OCM, including the correlations for all model parameters, was implemented into an existing single-cylinder GT-Power model as a user defined function [17]. In this particular case, the OCM was connected to the combustion object of the engine cylinder module (see Figure 8). Input data for the OCM, e.g. wall temperatures and heat transfer coefficient, are specified within the engine cylinder module and passed on to the combustion model.

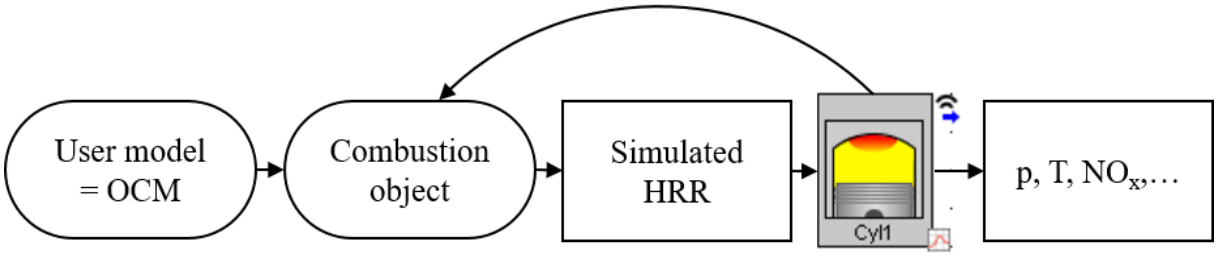

Figure 8. Implementation of the open chamber model in the single cylinder GT-Power model

RESULTS

Experimental results

An overview of measurement results for the hydrogen combustion system is provided in [3]. In this study the measurements were evaluated with a strong focus on the ignition phase, combustion phasing and combustion duration as well as cyclic variability. The ID was defined as

$$ID = MFB5\% - IT. \quad (6)$$

Burn duration (BD) is approximated as

$$BD = MFB90\% - MFB5\%. \tag{7}$$

Figure 9 shows key combustion metrics, i.e. ID, MFB5%, MFB50%, MFB90%, for ignition timing variations with different EAR at a high load engine operating condition. On the left-hand side average values of 60 consecutive combustion cycles are shown. Standard deviations (STD) are displayed on the right-hand side. The ID decreases with lower EAR and earlier IT (as expected). In contrast to the coefficient of variation (COV) of IMEP that was shown to increase with later ignition timing in previous studies, the standard deviation of the ID shows only a minor dependence on ignition timing and remains at a rather large value. The standard deviations of MFB50% and MFB90% increase with later IT and for leaner mixtures. Late MFB90% and high standard deviation might indicate that cycles with slow combustion exist.

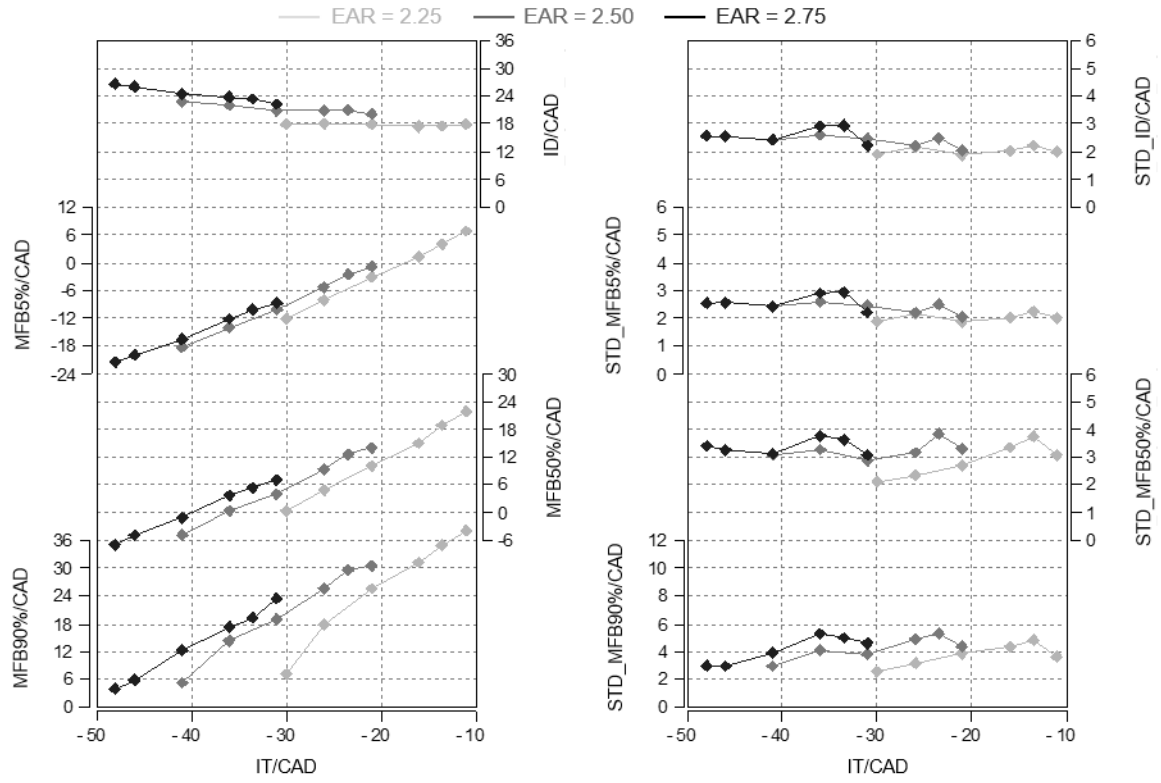

Figure 9. Combustion-related measurement data for high load operation at 1500 rpm

Analysis of individual cycles (Figure 10, left) shows that while MFB90% shows a wide spread, the combustion duration only varies in a narrow range from 27 to 31.5 CAD. Cycles with late MFB90% show a longer burn duration as is expected due to decreasing pressures and temperatures during the expansion stroke. But rather than being associated with a long burn duration cycles with late MFB90% have a long ID and late MFB5%. There is a strong correlation between MFB5% and MFB50% as well as between MFB5% and MFB90%. No individual cycles were observed where the combustion progressed slowly after a short ID and early MFB5%, leading to the conclusion that ignition phase offers the largest potential to reduce cyclic variability for hydrogen combustion.

Another indication that using hydrogen as a fuel leads to a larger spread in the combustion phasing can be seen in Figure 11. The data plotted in this figure comes from a different large bore gas engine with open combustion chamber. On the left-hand side key combustion

parameters for individual cycles in natural gas operation are shown, while on the right-hand side the results from hydrogen operation are displayed. Even though the ignition timing for the hydrogen operation is significantly later than for the natural gas operation, the spread of MFB5% and therefore ID is larger for the hydrogen operation. At this point it is unclear if the observed ignition behavior is mainly caused by the hydrogen properties or if mixture inhomogeneities also play a role.

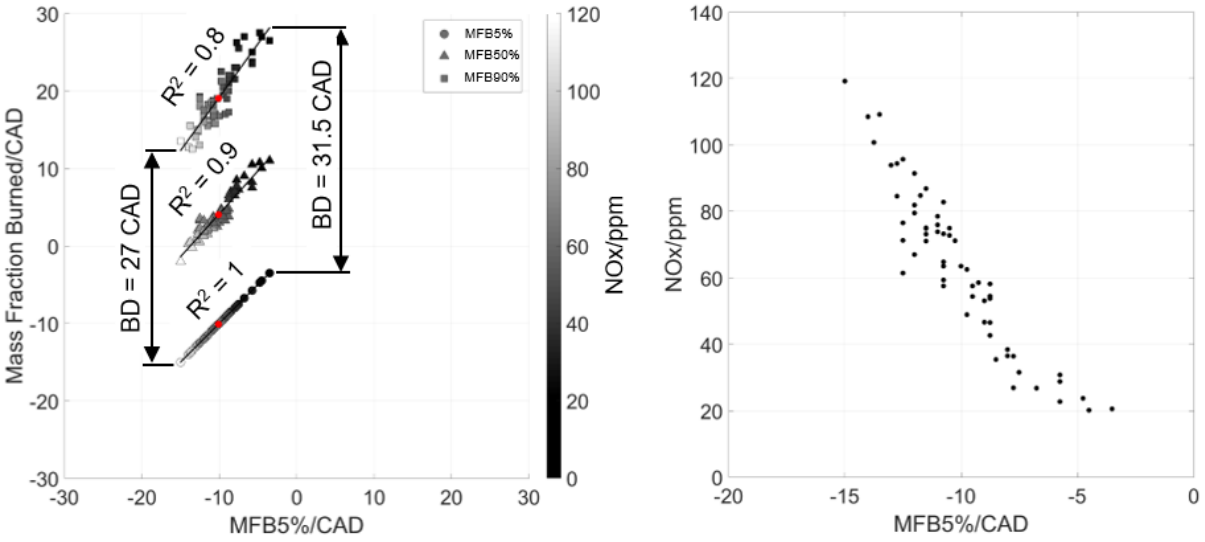

Figure 10. Individual cycle hydrogen combustion parameters (left) and calculated NO_x emissions (right) for high load operation at 1500 rpm (IT 31 CAD before TDC; EAR 2.5)

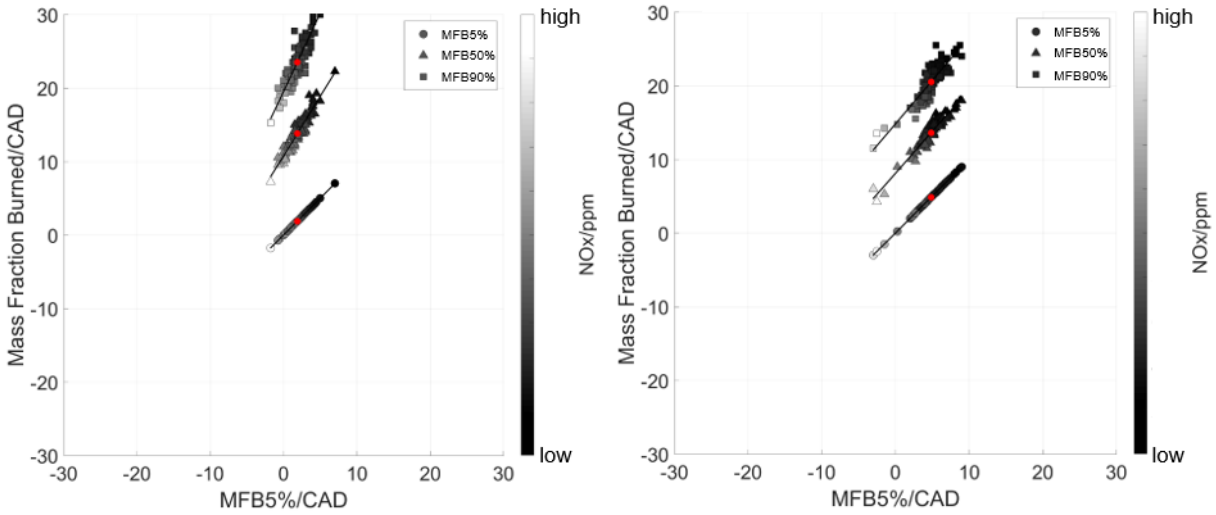

Figure 11. Individual cycle natural gas (left, IT 24 CAD before TDC) and hydrogen (right, IT 6 CAD before TDC) combustion parameters at constant MFB50%

Apart from the obvious drawbacks of high cyclic variability, the large variation in ID and combustion phasing might also limit the feasible operating range of hydrogen combustion. In Figure 10 (right) the NO_x formation is estimated for each individual cycle based on the HRR and displayed over MFB05%. The early combustion cycles disproportionately contribute to overall NO_x formation. A narrower spread of the ID and the combustion phasing could potentially facilitate a reduction of NOx emissions.

Numerical/Modeling results

High load operation. The performance of the OCM was evaluated based on comparisons of the simulated HRR with the HRR from the single cylinder engine measurements. The OCM was used as a stand-alone model and as a user model in the 1D performance simulation. Results for high load operation with early ignition timing and high EAR can be seen in Figure 12. The stand-alone simulation ("0D combustion simulation") is able to accurately predict the HRR while the 1D simulation shows some deviation despite the use of identical model parameters in both cases. The cause of the deviation are the differences in the OCM input parameters. The trapped mass, EAR and the mixture temperature at IVC are not imposed in the 1D simulation but the results of the gas exchange simulation and might differ from the measured values. The difference in the HRR between the two simulations is an indication of the model sensitivity to input and boundary conditions.

For the 1D simulation additional parameters were compared to the experimental results. The indicated efficiency showed a deviation of approx. 0.3 percentage points and the exhaust gas temperature differed by approx. 4 K.

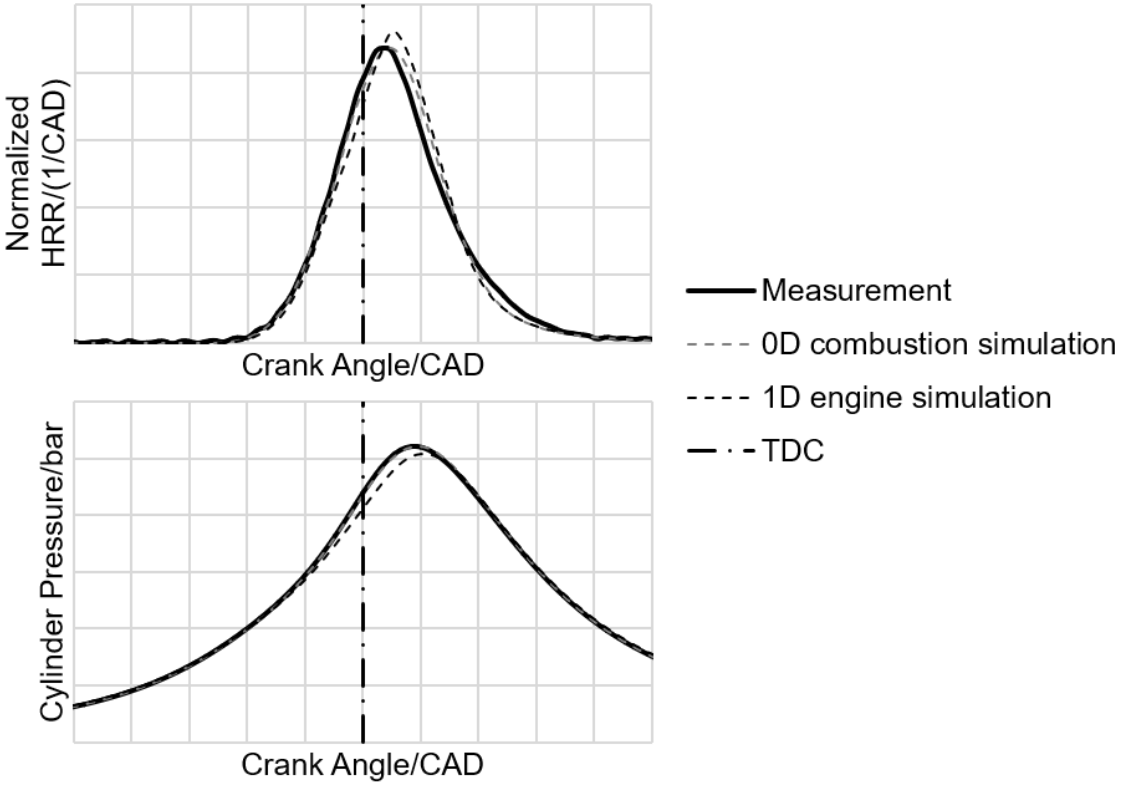

Figure 12. Comparison of experimental and simulated HRR and cylinder pressure for high load operation at 1500 rpm

Part load operation. The HRR for part load operation with an EAR at the lower limit of the investigated range are shown in Figure 13. In contrast to the high load condition major differences exist between experimental and simulated HRR and the differences between the two simulation models are more pronounced than for high load operation. The indicated efficiency for the 1D simulation showed a difference of approx. 1.7 percentage points to the measurement results.

Since the deviation in the HRR is apparent for both simulation cases differences in the input parameters cannot be the only cause of the deviations. The OCM is not able to predict the retarded combustion sufficiently well which could indicate that a physical process or parameter

is not accurately reflected in the model or that model parameters are not properly adjusted. The high cyclic variability discussed in the "Experimental results" and the fact that average HRR were used for model parameter adjustment could also contribute to the deviations.

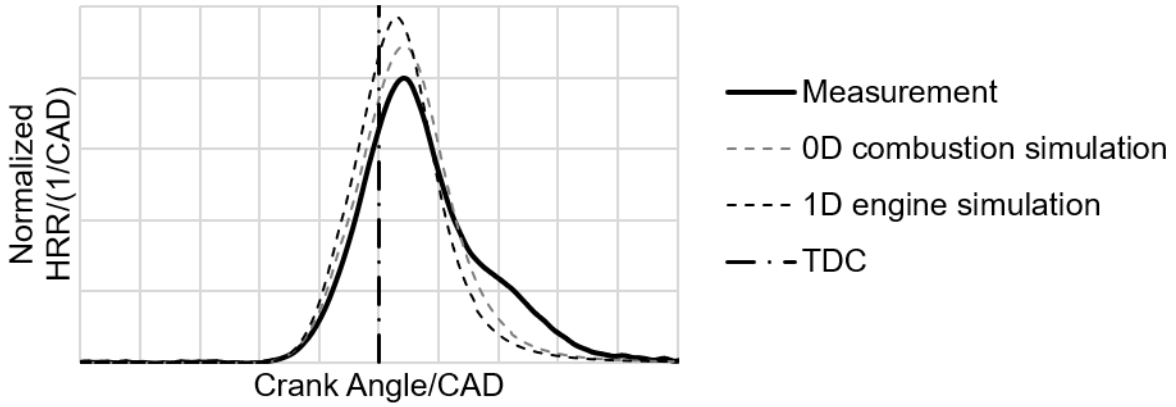

Figure 13. Comparison of experimental and simulated HRR for part load operation at 1500 rpm

CONCLUSION

In this study hydrogen combustion in a large-bore gas engine was investigated. Analysis of measurements from a single-cylinder research engine with an open combustion chamber and spark ignition revealed large cyclic variations in the ID and the subsequent main combustion phase. The cyclic variations in the main combustion phase are caused by the variation in the ID and not by large variations in the combustion duration. The ID variation seems to be particularly high with hydrogen fueling. An investigation of different ignition concepts, e.g. pre-chamber ignition or diesel pilot ignition, will be performed in a future study to evaluate the potential of hydrogen combustion in a large-bore engine. In order to eliminate mixture inhomogeneities as a possible cause for cyclic variations central mixture formation instead of port fuel injection should be investigated as well.

To facilitate HyMethShip reformer-engine system optimization a quasi-dimensional model for hydrogen combustion was developed and calibrated with averaged measurement data from single-cylinder experiments. LFS values were calculated using a chemical kinetics calculation tool in combination with an appropriate reaction mechanism. Evaluation of simulated HRR with measurement data showed that high load operation can be predicted with decent accuracy while the slower and retarded combustion at part load operation could not be depicted at all. A comparison of the stand-alone OCM and the 1D simulation model showed a strong sensitivity to input and boundary conditions. Therefore, the first attempt for combustion model improvement will include improving the accuracy of the model input parameters, e.g. fuel and air mass in the cylinder and mixture temperatures at IVC. Furthermore, the procedure for the model parameter adjustment needs to be revisited and possibly adjusted. Finally, a procedure needs to be defined to deal with measurement data with high cyclic variability. Usage of individual cycles or elimination of very early or very late cycles might be considered. Preferably the improvement of the ignition and combustion system will eliminate the high cyclic variation.

ACKNOWLEDGEMENT

This project has received funding from the European Union's Horizon 2020 research and innovation program under grant agreement No. 768945.

NOMENCLATURE

C_{ID}	Ignition delay factor
C_k	Turbulent kinetic energy factor
C_L	Integral length scale factor
C_{mod}	Combustion factor
CAD	Crank angle degree, Computer aided design
COV	Coefficient of variation
CR	Compression ratio
DF	Dual fuel
DI	Direct injection
$\mathrm{d}m_c$	Mass flow into burned zone
EAR	Excess air ratio
EOI	End of injection
EVO	Exhaust valve opening
HRR	Heat release rate
ID	Ignition delay
IMEP	Indicated mean effective pressure
IT	Ignition timing
IVC	Intake valve closing
k_{ivc}	Turbulent kinetic energy at IVC
L	Liter
l_I	Integral length scale
LFS	Laminar flame speed
L_{st}	Stoichiometric air-fuel-ratio
$\dot{m}_B$	Fuel mass flow
m_{ff}	Mass in flame front zone
$\dot{m}_L$	Air mass flow
MFB5%	Mass fraction burned 5 %
MFB50%	Mass fraction burned 50 %
MFB90%	Mass fraction burned 90 %
NG	Natural gas
OCM	Open chamber combustion model
p	Pressure
PFI	Port fuel injection
r_{fr}	Radial major axis of the ellipsoid
rpm	Revolutions per minute
SCE	Single cylinder engine
SI	Spark ignition
s_l	Laminar flame speed
SOC	Start of combustion
s_t	Flame speed
s_{t0}	Turbulent flame speed
STD	Standard deviation
T	Temperature
τ	Characteristic burn duration
TDC	Top dead center
V	Cylinder volume
w	Entry velocity

REFERENCES

[1] IMO webpage. “http://www.imo.org/en/MediaCentre/PressBriefings/Pages/06GHGinitialstrategy.aspx”, last access on March 2nd 2020.

[2] Zelenka, J., Wermuth, N., Lackner, M., et al., The HyMethShip Project: Innovative Emission Free Propulsion for Ships, Paper No. 104, 29th CIMAC World Congress Vancouver 2019.

[3] Wermuth, N., Lackner, M., Barnstedt, D., et al., The HyMethShip Project: Innovative Emission Free Propulsion for Maritime Applications, 17. FAD-Konferenz Dresden 2019.

[4] Kim, J., Chun, K. M., Song, S., Baek, H.-K., Lee, S. W., Hydrogen effects on the combustion stability, performance and emissions of a turbo gasoline direct injection engine in various air/fuel ratios, *Applied Energy*, Vol. 228, pp 1353-1361, 2018.

[5] Tutak, W., Jamrozik, A., Grab-Rogalinski, K., Effect of natural gas enrichment with hydrogen on combustion process and emission characteristic of a duel fuel diesel engine, *International Journal of Hydrogen Energy*, 2020.

[6] Yu, X., Li, G., Du, Y., et al., A comparative study on effects of homogeneous or stratified hydrogen on combustion and emissions of a gasoline/hydrogen SI engine, *International Journal of Hydrogen Energy*, Vol. 44, pp 25974-25984, 2019.

[7] Sapra, H., Godjevac, M., De Vos, P., et al., Hydrogen-natural gas combustion in a marine lean-burn SI engine: A comparitive analysis of Seiliger and double Wiebe function-based zero–dimensional modelling, Energy Conversion and Management, Vol. 207, 2020.

[8] Zhen, X., Li, X., Wang, Y., et al., Comparative study on combustion and emission characteristics of methanol/hydrogen, ethanol/hydrogen and methane/hydrogen blends in high compression ratio SI engine, *Fuel*, Vol. 267, 2020.

[9] Tüchler, S., Dimitriou, P., On the capabilities and limitations of predictive, multi-zone combustion models for hydrogendiesel dual fuel operation, *International Journal of Hydrogen Energy*, Vol. 44, pp 18517-18531, 2019.

[10] N. Peters, Turbulente Brenngeschwindigkeit, Institute for Combustion Technology, RWTH Aachen, 1994.

[11] Cantera webpage. “http://cantera.github.io/docs/sphinx/html/index.html”, last access on March 2nd 2020.

[12] Davis, S. G., Joshi, A. V., Wang, H., et al., An optimized kinetic model of H2/CO combustion, *Proceedings of the Combustion Institute*, No. 30, pp 1283-1292, 2005.

[13] University of Southern California Combustion Kinetics Laboratory webpage. “http://ignis.usc.edu/Mechanisms/Model%20release.html”, last access on March 2nd 2020.

[14] Auer, M., Erstellung eines phänomenologischen Modells zur Vorausberechnung des Brennverlaufes von Gasmotoren, *Magerkonzept-Gasmotoren Verbrennungsmodelle*, Forschungsheft 885, 2009.

[15] Zimont, V., Polifke, W., Bettelini, M., et al., An Efficient Computational Model for Premixed Turbulent Combustion at High Reynolds Numbers Based on a Turbulent Flame Speed Closure, *J. Eng. Gas Turbines Power*, Vol. 120, No. 3, pp 526-532, 1998.

[16] Bargende, M., Ein Gleichungsansatz zur Berechnung der instationären Wandwärmerluste im Hochdruckteil von Ottomotoren, *PhD Thesis*, University of Stuttgart, 1990.

[17] Gamma Technologies LLC, User Programming Manual, 2018.